Microchemical Journal 203 (2024) 110953

Contents lists available at ScienceDirect

Microchemical Journal

journal homepage: www.elsevier.com/locate/microc

Development of ultra-sensitive and label-free ellipsometric aptasensor for the detection of residual fipronil

Arzu Keske [a], Mustafa Oguzhan Caglayan [b], Zafer Üstündağ [a,*]

[a] Kutahya Dumlipinar University, Chemistry Department, Kütahya, Turkiye
[b] Bilecik Seyh Edebali University, Bioengineering Department, Bilecik, Turkiye

ARTICLE INFO

Keywords:
Fipronil
Insecticide
Aptamer
Aptasensor
Ellipsometry

ABSTRACT

Fipronil, an insecticide widely employed, poses risks to both the environment and human health. Existing detection methods for fipronil and its metabolites, such as GC–MS, are known; however, these methods are laborious and time-intensive. In this investigation, our aim was to devise a label-free aptasensor strategy for detecting fipronil in food-related scenarios. To achieve this objective, we developed ellipsometric-based aptasensors specifically tailored for fipronil detection. The advantage of ellipsometric sensors lies in their efficacy in analyzing thin and uniform films. Spectrophotometric ellipsometry (SE), utilized in this realm, is preferred due to its sensitivity to molecular accumulation at the substrate surface, as evidenced by the phase shift (Δ). The limit of detection (LOD) observed in the buffer solution for the two aptamers, Anti-FIP1 and Anti-FIP2, used in this study, with lengths of 80 and 73 bases respectively, showed promising results. Additionally, the specificity of these aptamers against bovine serum albumin and ethiprole in the SE sensor approached the reproducibility limit. This is attributed to the wide-ranging cocktail employed during the aptamer selection process. The LOD for Anti-FIP1 was 0.034 nM (33.7 pM), while for Anti-FIP2 it was 0.025 nM (24.9 pM). The limit of quantification (LOQ) was calculated as 0.1 nM (0.044 ng/mL) for Anti-FIP1 and 0.075 nM (0.033 ng/mL) for Anti-FIP2. Utilizing the spike method for fipronil detection by introducing egg and grain samples, the deviation observed was less than ±10 % for recovery. This study presents a dependable aptasensor platform for the testing of fipronil in food samples, employing aptamer-based SE.

1. Introduction

Fipronil is an insecticide with systemic properties, accounting for approximately 10 % of the global insecticide market volume [1]. Fipronil exhibits its insecticidal activity by inhibiting the nervous system, binding to γ-aminobutyric acid (GABA) receptors [2], and glutamate receptors associated with chloride channels [3], disrupting neural signaling in insects. Glutamate receptors are specific to insects, making fipronil more effective on invertebrates compared to vertebrates, and fipronil also shows low affinity for vertebrate receptors [4]. Fipronil is metabolized into a sulfone compound in mammals, and experiments have shown that it binds to human and rodent GABA receptors with approximately 6 times higher affinity [5]. It has been shown that fipronil metabolites retain bioactivity and toxicity in mammals, with a 10-fold higher potential at the GABA-gated chloride channel in mammals (for fipronil-desulfinyl), narrowing the selectivity between insects and mammals [6]. Furthermore, despite the low affinity of fipronil for the natural mammalian heterooligomeric receptor compared to insect $GABA_A$ receptors, it has been found to have a high affinity for the human receptor subunit β3 [7]. The human β_3 $GABA_A$ receptor is associated with neurodevelopmental disorders such as autism, Angelman syndrome, and epilepsy [8]. Fipronil can affect some cytochrome P450 enzymes, and *in vitro* cytotoxic effects at high concentrations suggest toxicity potential through non-neural mechanisms [9]. Acute fipronil toxicity in laboratory rodents is characterized by tremors, altered activity or gait, hunched posture, agitation, seizures, and mortality at doses higher than 50 mg/kg [10]. Fipronil toxicity indications in humans, are characterized by increased excitability, headaches, dizziness, seizures, decreased food consumption, nausea, and vomiting, independent of neural targets [9]. Additionally, a range of significant risks for the environment has been identified, including acute and chronic risks to freshwater and marine invertebrates and fish species, acute lethal and reproductive risks for birds, and reproductive effects in insectivorous mammals [9].

* Corresponding author.
E-mail addresses: zustundag@gmail.com, zafer.ustundag@dpu.edu.tr (Z. Üstündağ).

https://doi.org/10.1016/j.microc.2024.110953
Received 25 April 2024; Received in revised form 6 June 2024; Accepted 7 June 2024
Available online 8 June 2024

Fipronil remains stable under acidic and neutral conditions [11] and the half-lives of fipronil and its metabolites under aerobic soil conditions can vary significantly but are generally a few months. It is indicated that people worldwide are exposed to fipronil via contaminated water sources [12] even contaminated food sources such as honey [13]. Extensive information on the physicochemical properties of fipronil, along with its environmental fate, can be found in the literature [13]. Hence, the EPA has classified fipronil as a moderately toxic potential human carcinogen and has established a range of restrictions for residue concentrations for different products, ranging from 0.005 to 1.5 ppm (Title 40 of the Code of Federal Regulations: Protection of Environment, PART 180—TOLERANCES AND EXEMPTIONS FOR PESTICIDE CHEMICAL RESIDUES IN FOOD Subpart C—Specific Tolerances, §180.517; https://www.ecfr.gov/) [14].

Detection of residues of fipronil and its metabolites in environmental samples and body fluids is typically carried out using well-known analytical techniques such as liquid chromatography (LC) or gas chromatography (GC) coupled with sensitive and highly selective mass detectors [15–20]. Some chromatographic methods encountered in the literature and their analytical performances are summarized in Table 1. Despite the advantages of being highly sensitive and selective, instrumental methods require extensive sample preparation and cleanup

Table 1
Comparison of some fipronil detection methods.

Method	Sample	Linear range	LOD	References
^{19}F – qNMR (with dispersive liquid–liquid micro-extraction)	Egg	NR*	57 nM	[21]
Colorimetric (AgNP, LFIA, pAb)	Egg, honey, tea, urine	NR*	6.9 nM (instrumental)	[22]
Colorimetric (AuNP, LFIA, mAb, indirect competetive ELISA)	Egg, cucumber	NR*	0.114 nM	[23]
Colorimetric, aptamer	Water, soil vegetable	NR*	0.036 μM	[24]
Colorimetric, LSPR, peptide aptamer, AuNP	Egg	2.3 pM–2.3 μM	22.9 pM	[25]
ECL	Egg	1–100 μM	0.8 μM	[26]
ECL (ZnO @ g-C_3N_4, GCE)	Egg	5–1000 nM	1.5 nM	[26]
Electrochemical (Al-TiO_2, GPE)	Egg	23–206 pM	38 pM	[27]
Electrochemical (CoZnO nanofiber) mAb	Egg	0.23 fM–228 μM	0.26 fM	[28]
Electrochemical (FeO.TiO_2, CPE)	Egg	1–100 nM	1.2 nM	[29]
Electrochemical (nanocomposite on SPE)	Egg	1.0–8.0 μM	0.74 μM	[30]
Electrochemical (nanocomposite, aptamer, GCE)	Water	0.23–22.8 μM	0.17 nM	[31]
Electrochemical (SPE, nanocomposite, aptamer)	Honey	NR*	2.45 nM	[32]
Electrochemical (SPE, nanocomposite, immunoassy)	Agricultural products	0.23–2.3 μM	48 pM	[33]
Electrochemical (SPE, TiO_2, polytriazine imide, CoZnO nanofiber)	Egg, water	0.01–10 μM	8.42 nM	[34]
Electrochemical (TiO_2, CPE)	Egg	1 pM–100 nM	0.34 nM	[35]
Electrochemical, CPE	Milk	NR*	0.76 nM	[36]
ELISA	Animal tissue	68 nM–2.28 μM	23 nM	[37]
ELISA	Water samples	0–1.14 μM	52 nM	[38]
ELISA	Urine, serum	NR*	1.33 nM	[9]
ELISA, TRFICA	Chinese cabbage, spinach, apple and egg	NR*	1.97 nM	[39]
Fluorescence (aptamer)	Egg	5–500 nM	105 nM	[40]
Fluorescence	Egg, milk	0.70 pM – 47 μM	19 pM	[41]
Fluorescence (aptamer)	Egg	72–864 nM	155 nM	[42]
Fluorescence (aptamer)	Plant tissue extracts	5–65 nM	3.4 nM	[43]
Fluorescence (aptamer), oxidized carbon nanohorns	Egg	NR*	3 nM	[44]
Fluorescence (immunoassay, FRET, upconversion NPs)	Spinach	22.8–228 nM	0.01	[45]
Fluorescence (nanocomposite, FRET, aptamer)	Egg	10–60 nM	3.6 nM	[46]
Fluorescence, competitive immunoassay	Water samples	57–373 pM	41.1 pM	[47]
Fluorescence, evanescent wave	Milk, water	NR*	73 pM	[48]
Fluorescence, metal organic framework	Tea	0–0.15 mM	4.4 nM	[49]
GC-ECD	Water	0.46–228 nM	46 pM	[50]
GC-ECD	Edible oils	4.6–457 nM	0.46 nM	[51]
GC-ECD	Edible oils	1.81–904 nM	0.54 nM	[52]
GC-ECD	Honey	NR*	2.29 nM	[53]
GC–MS	Water, soil, urine	0.686–229 nM	0.18 nM	[54]
HPLC	Water samples	114 pM–45.8 nM	18.3 pM	[55]
LC-MS/MS	Egg	NR*	0.8 nM	[56]
LC-MS/MS	Water samples	114 fM–0.229 nM	45.8 fM	[57]
LDI-MS	Blueberry juice, green tea beverage, fish muscle	0.46–229 nM	0.11 nM	[58]
Luminescence	Egg	1–100 μM	0.8 μM	[59]
Raman	Egg	2.3 μM-1.1 mM	0.73 μM	[60]
SERS	Egg	0.23 nM–228 nM	2.3 nM	[61]
SERS (aptamer)	Egg	100 nM-100 μM	100 nM	[62]
SERS (Au nanorods, graphene oxide enhancer)	Egg	10 nM–100 μM	10 nM	[63]
SERS, nanocomposite	Water	NR*	228 nM	[64]
SERS-RRS	Egg	11.4 pM – 1.14 nM	11.4 pM	[65]
UHPLC-MS/MS	Egg	2.3–45.8 nM	0.69 nM	[66]
UHPLC-MS/MS, various extraction strategies	Egg	NR*	0.69 nM	[67]
UHPLC-Q-Exactive HRMS, nanocomposite	Egg	NR*	4.5 pM	[68]
Spectroscopic ellipsometry (aptamer 1)	Egg, grain	0.1–1000 nM	33.7 pM	This study
Spectroscopic ellipsometry (aptamer 2)	Egg, grain	0.1–1000 nM	24.9 pM	This study

NR* – Not reported.

ECL – Electrochemiluminescence, GCE – Glassy carbon electrode, GC-ECD – Gas chromatography-electron capture detection, GPE – Graphene paste electrode, LC-MS/MS – Liquid chromatography-tandem mass spectrometry, LDI-MS – Laser desorption/ionization mass spectrometry, LFIA – Lateral flow immunoassay, LSPR – Based on localized surface plasmon resonance, mAb – monoclonal antibody, NPs – Nanoparticles, pAb – polyclonal antibody, qNMR – Quantitative nuclear magnetic resonance spectroscopy, SERS – Surface enhanced Raman scattering, SERS-RRS – SERS-Resonance Rayleigh scattering, SPE – Screen printed electrode, TRFICA – Time-resolved fluorescent immunochromatographic assay, UHPLC-MS/MS – Ultra high-performance liquid chromatography coupled with mass spectrometry, UHPLC-Q-Exactive HRMS – UHPLC coupled with Q-Exactive high resolution mass spectrometry.

procedures that can become cumbersome, time-consuming, and expensive, especially when analyzing a large number of samples in pollution monitoring studies.

Therefore, studies have been conducted for the detection of fipronil using different approaches including competitive-indirect enzyme-linked immunosorbent assays (ELISAs), fluorescence assays, colorimetric methods, vibrational spectroscopic methods, and electrochemical methods (Table 1). The majority of the studies reported in this table meet the detection limit (LOD) for fipronil concentration, which is the lowest legal residual limit of 11.4 nM. However, the LC_{50} limit of 74 fM reported for some species in insects for fipronil is well below these detection limits [29]. When only residues are considered, there is still a need for the development of an easier, more specific, and lower detection limit method.

Originally reported by Ellington and Gold, aptamers are sequences of single-stranded DNA or RNA (more recently, peptides) capable of adopting specific three-dimensional structures that allow them to bind specifically to their targets [69,70]. Aptamers are produced through the process known as Systematic Evolution of Ligands by EXponential enrichment (SELEX), involving target-specific enrichment [70]. Theoretically, they can be tailored for virtually any specific target. Over time, a diverse array of high-affinity aptamers has been developed for various target molecules, spanning from metal ions and peptides to drugs, proteins, and even entire cells or viruses [71].

A specific aptamer for fipronil (with a Kd = 48 ± 8 nM) exhibits positive selectivity for fipronil against to interfering agents atrazine, propanil, malathion, and ethiprole has been reported [40]. Additionally, another aptamer with similar motifs, but without specified kinetic performance, has been considered a promising alternative for fipronil detection in the same study [40]. In this study, the aim was to use the two alternative fipronil-specific aptamers that have been reported for their selectivity in fipronil detection and to evaluate their analytical performance.

Elipsometry is a method that measures the phase difference and intensity of polarized beams of monochromatic light reflected from thin films. Parameters Δ (Delta) for phase and Ψ (Psi) for intensity of polarized light are measured with respect to the wavelength of the incoming light (spectroscopic ellipsometry). Δ and Ψ are functions of the refractive index and thickness of the medium interacting with the reflected light on the surface [72]. By measuring these parameters from nanofilms on a substrate material, the accumulation on the surface can be precisely quantified [73,74]. Various studies have evaluated the performance of ellipsometry in different analytes. The use of aptamers and ellipsometry has been reported in the determination of aminoglycoside antibiotics in dairy products [75], HIV-1 Tat protein detection [76], Influenza A detection [77], mercury ion detection [78], and zearalenone determination [79], among others. Fig. 1 provides a schematic representation of the ellipsometric fipronil sensor.

In this study, two aptasensor platforms based on spectroscopic ellipsometry (SE) were developed for the first time for the detection of fipronil. The performance of these platforms in detecting fipronil, including real samples, was investigated.

2. Experimental

2.1. Chemicals

Analytical grade fipronil (FIP) was utilized for surface functionalization, alongside mercaptopropyltriethoxysilane (MPTES, 97 %), mercaptoundecanoic acid (MUA), ethanol, acetonitrile, hexane, and

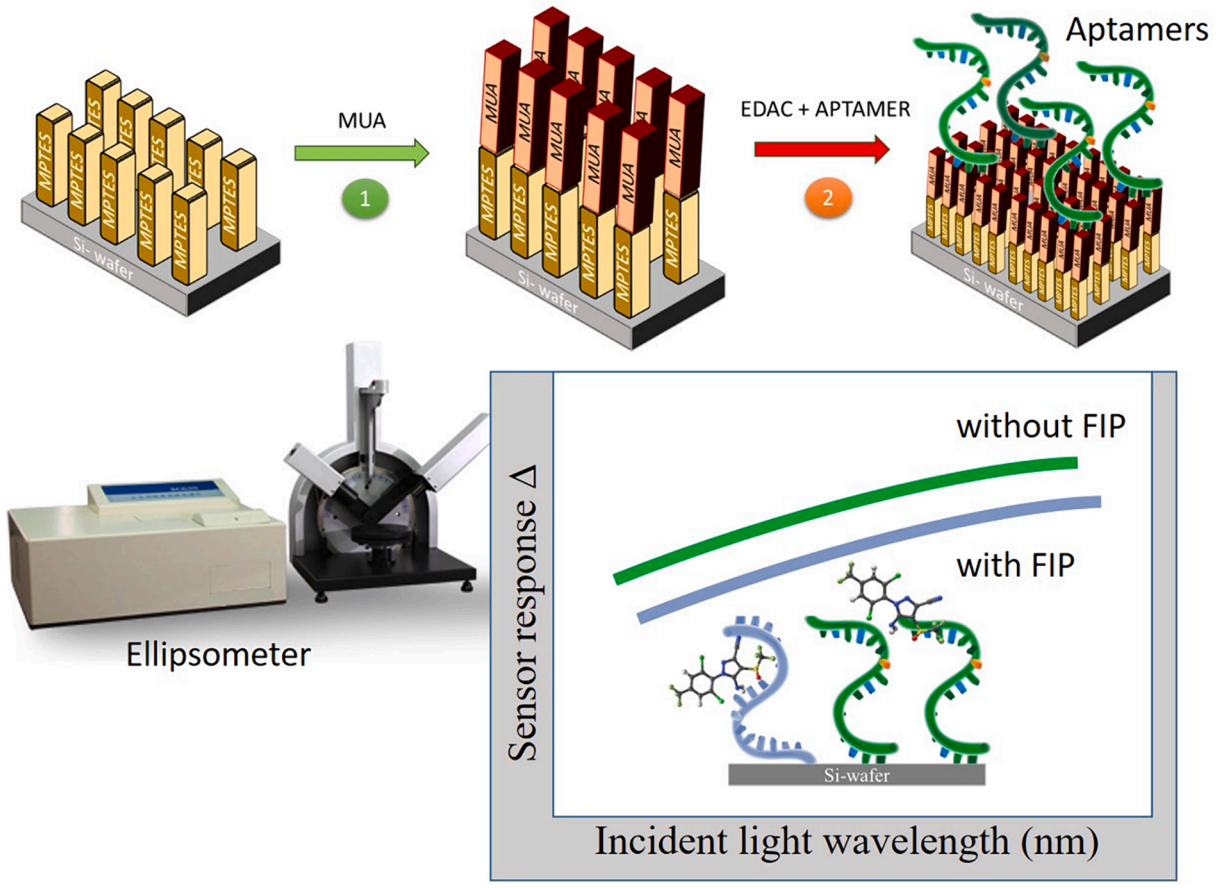

Fig. 1. Schematic representation of the ellipsometric sensor platform (Si chip with immobilized aptamer, ellipsometer setup, and typical sensor data obtained during binding).

ammonia. NaH_2PO_4 and Na_2HPO_4 were employed for buffer solutions. Aptamer sequences were obtained with a 5′ modification (amine). All chemicals and aptamers were purchased from the local representatives of Merck or Sigma-Aldrich and were used without further processing unless specified otherwise. Measurements were conducted using a spectroscopic ellipsometer (Optosense S9000, Turkey). Si chips served as the base material for surface modification, with the optical properties (and thicknesses) of the accumulated organic matter on these surfaces determined via ellipsometry. A phosphate buffer at pH 7.4, with a concentration of 100 mM, was prepared for the experiments.

2.2. Modification of the Si-wafers

The attachment of the aptamer, which was thiol-functionalized, onto the Si surface was achieved through the formation of an S-S bond with the MPTES-functionalized surface [80]. Anti-fipronil aptamers, specifically modified with an amino group at their 5′ ends for immobilization onto Si chips, were sourced from the local representative of TIB MOLBIOL (Germany). The aptamers utilized in this investigation are detailed in Table 2. Before usage, the Si chips employed as the sensor substrate were dipped into an oxidizing solution comprising H_2SO_4 and H_2O_2 (v/v 7:3) for 2 s, followed by rinsing with ethanol. Subsequently, for the complete elimination of any organic residues, they underwent a cleaning process using oxygen plasma at 100 W power with a Diener (Germany) model plasma device.

The Anti-FIP1, Anti-FIP2, and control (FIPCTRL) aptamers were attached onto the Si chip surfaces terminated with –COOH groups. To achieve this, Si chips of approximately 1 cm × 1 cm dimensions were cut and thoroughly cleaned. These cleaned chips were then subjected to oxygen plasma for 30 min to induce a silanol reaction. Subsequently, MPTES dissolved in absolute ethanol was utilized to create a functional surface with −SH terminations on the Si chips. During the formation of the MPTES layer, the optimization of MPTES concentration and reaction duration was carried out through ellipsometric thickness measurements. Next, the –COOH functional groups were established on the Si chip surfaces using MUA via a disulfide reaction. The process of layer formation was monitored at this stage by measuring the ellipsometric thickness to determine the optimal parameters. Following this, the aptamers containing NH_2 functional groups were immobilized onto the –COOH functionalized Si surfaces using the 1-ethyl-3-(3-dimethylaminopropyl) carbodiimide (EDAC) reaction. These aptamers were prepared in a 100 mM phosphate buffer solution (PBS, pH 7) and stored at 4 °C. The aptamer solutions used in the experiments were prepared by dilution from the stock solution. The optimization of concentration and reaction times involved determining the thickness of the organic accumulation on the Si chip surfaces using ellipsometric methods. The ellipsometric measurements were modeled using the device's software, considering a model of air/organic layer (with the measured thickness)/SiO_2 layer (5 nm), and Si substrate. The concentrations mentioned in the study indicate the final concentrations used. All experiments and measurements were repeated three times unless otherwise specified to meet the analytical requirements.

Table 2
Fipronil aptamers used in this study.

Sequence	Name	Reference
5'-TGTAC CGTCT GAGCG ATTCG TAC AGTTT CTGGA GGACT GGGCG GGGTG ACGGT TATG AGCCA GTCAG TGTTA AGGAG TGC-3'	Anti-FIP1	[40]
5'-CCGTC TGAGC GATTC GTACC AAAGT CGAGA CTGTA GTGAG GCAAA AAGCC GGCAG CCAGT CAGTG TTAAG GAG-3'	Anti-FIP2	[40]
5'-ACCTG CAGGC GCGAG TTTCA GATCA AAACT TGTCT GGCGT-3'	FIPCTRL	None

2.3. Ellipsometric measurements

The analytical performance of aptamers Anti-FIP1, Anti-FIP2, and FIPCTRL in detecting FIP was assessed using FIP solutions ranging from 100 pM to 1000 nM in a buffer solution. The FIP solutions were prepared using PBS buffer (pH 7.4, 150 mM NaCl). The ellipsometric measurements were performed using a spectrophotometric ellipsometer with light at incident angles of 60° and 70° and wavelengths ranging from 400 to 1700 nm. The ellipsometric parameters, delta (Δ) and psi (Ψ), were obtained, and the sensor response was analyzed based on the change in Δ and Ψ values. Delta (Δ) indicating the phase shift between the polarized incident light and the reflected light, was chosen as the preferred sensor response due to its sensitivity to the accumulated material on the surface, affecting its thickness and dielectric function. The Δ spectrum obtained around 450–600 nm exhibited a nearly linear change, shifting towards lower degrees with increased accumulation on the surface. Therefore, sensor calibration graphs were generated using the Δ values at this wavelength. The sensitivity and LOD were calculated from the graph depicting Δ changes concerning FIP concentrations using 3σ as noise level. Quantification limits (LOQ) were calculated using 3×LOD approach. To assess specificity, interference experiments were conducted with BSA and another broad-spectrum insecticide, ethiprole.

The thickness of the molecular layer accumulated on each sensor chip's surface was calculated using both Δ and Ψ values with the model solver software of the ellipsometer. All thickness measurements were conducted on ten different randomly selected measurement points on three distinct test samples, and the average value (±1σ) was reported.

2.4. Fipronil detection in food samples

The food samples were prepared following the procedures outlined in the literature [81]. The extraction protocols specified for solid food samples were applied accordingly [41]. Acetonitrile was used for the extraction of both sample types, and 0.22 μm syringe filters were employed to eliminate any impurities from the resultant mixtures. Local market-sourced egg samples were used in the study. For standard addition, a specific quantity of fipronil and 10 mL of acetonitrile were added to 5 g of homogenized sample. Subsequently, 4 g of anhydrous $MgSO_4$ and 1 g of NaCl were introduced to the homogenized mixture, which was thoroughly mixed. Following this, it underwent centrifugation at 5000 rpm for 10 min. The supernatant was then evaporated in a 25 mL beaker at room temperature and subsequently reconstituted in 5 mL of 0.1 M PBS (pH 7.4). This resulting solution was filtered through a 0.22 μm filter and diluted to 25 mL using PBS buffer prior to analysis [26,41]. The recovery efficiency was calculated by determining the ratio between the fipronil concentration obtained from the calibration curve and the corresponding fipronil concentration artificially added to the blank sample [60].

The grain (wheat) samples used in the study were sourced from a local market. Before processing, the samples underwent a drying process at 80 °C for 2 days [82]. Subsequently, 20 g of the dried grain samples were pulverized, and then mixed with a specified amount of fipronil and 20 mL of acetonitrile. This mixture was then homogenized thoroughly. Following centrifugation, the resulting supernatant was carefully separated and combined with 4 g of anhydrous $MgSO_4$ and 1 g of NaCl. The mixture was then centrifuged once more at 5000 rpm for a duration of 10 min [83]. The supernatant obtained was dried in a 25 mL beaker at room temperature and later dissolved in 5 mL of 0.1 M PBS (pH 7.4). The solution was subsequently filtered using a 0.22 μm filter, diluted to a volume of 25 mL with PBS buffer, and prepared for analysis.

3. Results and discussion

3.1. Modification of Si-wafers

Firstly, the conditions for the immobilization of the MPTES layer on

the Si wafer were optimized. The effect of the interaction time on surface accumulation was investigated using Si wafers treated with oxygen plasma in a 1 μM MPTES solution for varying durations. The surface thickness measured by ellipsometry after this process ranged up to a maximum of 1.8 nm within the first 120 min. For 240 and 360 min, the thickness values increased to around 2.7 nm (See Fig. S.1). It has been noted that MPTES molecules yielded ellipsometric results higher than their theoretical lengths in previous studies (approximately 3 nm) [80]. However, considering the theoretical length (~1 nm), it can be said that a nearly single-layer formation occurred within the initial 120 min, and thereafter, multiple layers (oligomeric form) were formed by 240 min [84]. Therefore, the reaction carried out with 1 μM MPTES for 120 min was deemed sufficient and appropriate for the objectives of the study.

Subsequently, optimization was carried out to create a disulfide bond between the −SH terminated surface and MUA. For this purpose, the reaction was conducted at room temperature and in the dark. Considering the slow formation of the disulfide bond in our previous studies, the reaction was aimed to be carried out for 2 to 12 h to perform the time optimization. In this optimization phase, 1 μM MUA (in ethanol) was prepared. After the specified time, the previously MPTES-modified Si wafers were removed, washed with ethanol, and the accumulated layer on the surface was ellipsometrically measured. It was observed that with the use of 1 μM MUA, the thickness reached an approximate plateau after 6 h, which was considered as the optimal value (See Fig. S.2). The optimum binding time and concentration of aptamers with approximately the same base count (one with 80 and the other with 73 bases) were also determined as 120 min and 1.5 μM, respectively, by ellipsometric thickness measurements.

4. SE measurements and analytical performance of the sensor platform

Using spectroscopic ellipsometry, the interaction between the fipronil solution in the buffer and the Anti-FIP1, Anti-FIP2, and FIP-CTRL aptamers was investigated. For this purpose, the incident light angle was set to 60°, and the Δ change between 400 nm and 1700 nm was examined.

The sensor responses obtained by interacting the fipronil solution prepared in the buffer at different concentrations with the sensor chip were presented in average (line) and standard deviation (area) for convenience. It can be observed that the sensor response obtained from each sensor chip shows similarity (due to the base material being Si wafers and the top layer being organic material) and shifts to lower Δ degrees with increasing fipronil concentration (Fig. 2a and b). Furthermore, the Δ-λ change around 450–650 nm wavelength was found to be linear with a determination coefficient of >0.90 (in terms of R^2). This region also corresponds to the area where ellipsometric data follow approximately the same slope.

Within the range used to obtain the sensor response, all responses for the Anti-FIP1 aptasensor follow an average slope of 0.0167 ± 0.0022, and for the Anti-FIP2 aptasensor, it is 0.01683 ± 0.0007. Considering that the obtained standard deviation (0.0022) is only about 1 % of the average slope, the intersection point results of the curve fitting process were used to create the sensor calibration curve.

Relative sensor response (calculated based on the value measured when there is no fipronil present) was determined considering the linear region in this range, and the sensor calibration curve was established (Fig. 3a and b).

The calibration curves for Anti-FIP1 and Anti-FIP2 were obtained as straight lines fitting the equations $\Delta = 2.9739 \times \log [FIP] + 5.3369$ ($R^2 = 0.97$) and $\Delta = 1.36311 \times \log [FIP] + 2.7783$ ($R^2 = 0.98$), respectively (See Figs. S4 and S5). The noise levels, represented on the graph, were obtained by taking three times the standard deviation of the sensor signal for 10 nM fipronil for Anti-FIP1 (with a standard deviation of 0.32) and 1 nM fipronil for Anti-FIP2 (with a standard deviation of 0.20). Considering these noise levels, the LOD was determined as 0.034 nM (33.7 pM) for Anti-FIP1 and 0.025 nM (24.9 pM) for Anti-FIP2.

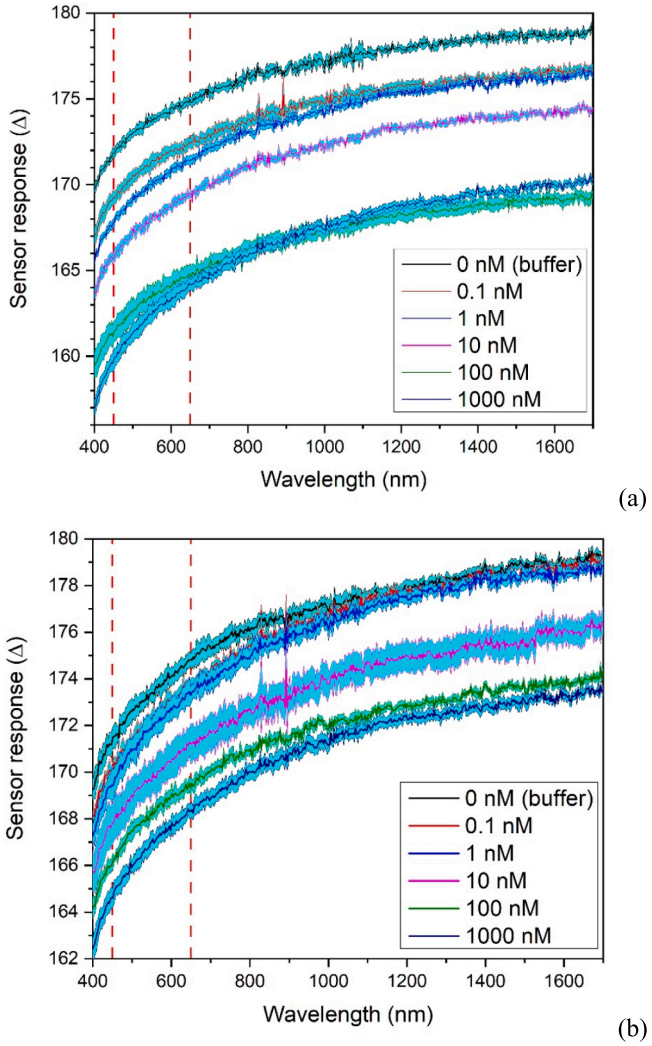

Fig. 2. a) Sensor response for Anti-FIP1 and b) Anti-FIP2 aptasensors for fipronil concentrations ranging from 0.1 nM to 1000 nM. The region where the calibration curve was generated is indicated by dashed red vertical lines. (For interpretation of the references to colour in this figure legend, the reader is referred to the web version of this article.)

The FIP-CTRL aptamer yielded a Δ change of 0.71 ± 0.23 when 100 pM FIP was used, 1.21 ± 0.42 Δ when 10 nM FIP was used, and 1.29 ± 0.37 Δ when 100 nM FIP was used. This indicates the selectivity of the aptamers and suggests that even a very low amount of fipronil could not be completely removed from the sensor surface during the washing step.

The relationship between the binding of captured fipronil from the solution to the aptamer on the sensor surface occurring at a single site, and the decrease in binding rate depending on the free aptamer concentration, was considered. In this regard, the conformity of the calibration data to the Langmuir model was also checked (See Figs. S6 and S7). The fipronil analyses conducted with both Anti-FIP1 and Anti-FIP2 aptamers respectively conform to the Langmuir model with determination coefficients of 0.992 and 0.998.

The Langmuir model coefficients are provided in Table S3. It was determined that the sensitivity of the AntiFIP1 sensor is higher than that of the Anti-FIP2 sensor. This result yields significant findings in terms of comparing the interaction between aptamer and fipronil in the Langmuir coefficients. The product of the parameters a and b is 5.92 for the AntiFIP1 model, while it is 2.92 for the Anti-FIP2 model.

Accordingly, the similarity in the c coefficients has raised the idea

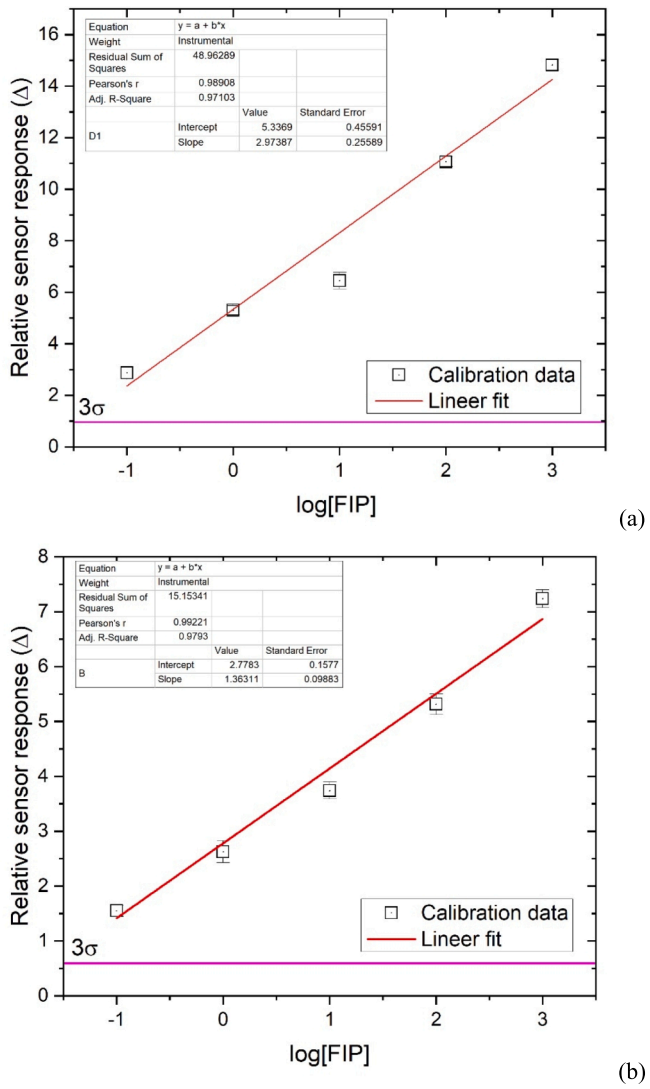

Fig. 3. Calibration curve obtained for Anti-FIP1 (a) and AntiFIP-2 (b) for fipronil concentrations ranging from 0.1 nM to 1000 nM.

that both aptamers capture fipronil through the same interaction site(s). Calculated from the DNAFold data (given in 5′ to 3′ base indices), the potential binding loops for both aptamers were as follows [85]: 1) For Anti-FIP1, a 3.15 kcal/mol hairpin loop between bases C_{65}-G_{75} (11 bases), a 3.42 kcal/mol internal loop between C_9-G_{48} (17 bases), and a 3.41 kcal/mol hairpin loop between T_{26}-A_{36} (11 bases). 2) For Anti-FIP2, a 3.04 kcal/mol internal loop between bases G_{33}-C_{57} (9 bases), a 0.84 kcal/mol internal loop between G_{38}-C_{53} (7 bases), a 2.10 kcal/mol hairpin loop between C_{42}-G_{48} (7 bases), and a 3.03 kcal/mol hairpin loop between G_{16}-C_{26} (11 bases).

Considering the base numbers and free energies, it can be observed that the 3.41 kcal/mol hairpin loop between T_{26}-A_{36} (11 bases) for Anti-FIP1 and the 3.03 kcal/mol hairpin loop between G_{16}-C_{26} (11 bases) for Anti-FIP2 are similar. This hairpin loop for Anti-FIP1, consisting of 4 Thymines, 4 Guanines, 2 Adenines, and 1 Cytosine, forms a loop with a stem connection of G-C pairs. Similarly, the loop for Anti-FIP2, containing 2 Thymines, 2 Guanines, 4 Adenines, and 2 Cytosines, also exhibits a similar connection. Additionally, in the Anti-FIP1 aptamer, the hairpin loop between C_{65}-G_{75} also consists of 3 Thymines, 4 Guanines, 3 Adenines, and 1 Cytosine.

Moreover, if Anti-FIP1 had two binding sites, it would be expected to affect the c coefficient in the model. However, despite the presence of two active regions in Anti-FIP1, the preference for the 11-base hairpin loops as the active fipronil binding regions might be indicated by the product of the Langmuir model's a and b parameters being 5.92 for the Anti-FIP1 model and 2.92 for the Anti-FIP2 model, where the preferential selection could be lower.

Although the Kd values for the aptamers were not disclosed in the selection paper [40], the interaction between the aptamer and FIP demonstrated an excellent fit to the Langmuir model, validating the anticipated single-site (1 aptamer − 1 FIP) relationship.

5. Specificity, accuracy and reproducibility tests

To test the specificity of the sensor, ethiprole (ETH) and bovine serum albumin (BSA) were used as interfering materials at concentrations of 10 nM and 1000 nM while testing the 1000 nM fipronil solution. The effect of the selected interfering agents at different concentration ratios on the sensor response is presented in Table 3.

In all measurements with the interfering components, a positive bias was obtained. The sensor response exhibited positive biases in all measurements due to nonspecific interactions, which also affected the standard deviation in the measurements. When the same ratio and a 100-fold concentration of the interfering component were used, both BSA biases for Anti-FIP1 and Anti-FIP2 were lower than the ETH bias. This may have occurred due to the structural similarity of ETH to fipronil. BSA, being a relatively large molecule, led to a low level of nonspecific interaction for both aptamers. The small biases in the sensor signal, reflected in the measured concentration due to the logarithmic structure of the calibration curve, were higher at higher fipronil concentrations. However, under all conditions, BSA interference ranged from 4.2 % to 7.7 %. This deviation is within the repeatability limits of the sensor.

In the case of ETH interference, the deviations were 7.3 % for the 10 nM fipronil measurement and 12.0 % for 1000 nM ETH. The excess deviation observed at higher concentrations can be associated with the logarithmic change in the calibration curve. While ETH shows a higher deviation compared to BSA when 10 nM fipronil and 1000 nM of the interfering substance are added, directly comparing this value (7.3 %) to the selectivity of the aptamer may not be realistic as it is still close to the repeatability limit.

For the use of ETH with the Anti-FIP2 aptamer, the deviation values were found to be 8.6 % and 12.7 %, respectively. Although this value is relatively high, it does not show a significant difference that can be attributed to selectivity.

Based on these reasons, it can be concluded that ethiprol either causes very low interference or no interference at all. In the article where the aptamers were selected, the authors have already verified the specificity of the selected aptamer for various interferents [40]. Among these interferents are fipronil metabolites; some herbicides and insecticides such as atrazine, which has a wide range of use, malathion, and propanil; and bovine serum albumin (BSA) as a general protein model.

The accuracy and precision of SE sensors using Anti-FIP1 and Anti-FIP2 aptamers were evaluated using 10 nM and 1000 nM fipronil solutions. For intra-day measurements, five independent sensor chip series were used. For inter-day measurements, five consecutive days each with five independent chip series were tested. The accuracy and precision of both methods are provided in Table 4.

The accuracy of the methods for intra-day measurements ranged from −8.54 % to −3.10 % for Anti-FIP1 and from −1.17 % to +0.3 % for Anti-FIP2. In inter-day measurements, the accuracy ranged from +6.9 % to +9.6 % for Anti-FIP1 and from +9.3 % to +9.6 % for Anti-FIP2. Due to the logarithmic nature of the calibration curve, small changes in sensor signal had a significant impact on the calculated results in inter-day accuracy, reaching up to 9.6 % for 1000 nM fipronil detection. However, the standard deviation for all measurements was quite low, with a maximum deviation of 0.22 % in precision.

For Anti-FIP2 aptamer, the intra-day accuracy ranged from −1.17 %

Table 3
Changes observed in the sensor signal obtained by measuring the fipronil added to the sample at concentrations of 10 nM and 1000 nM with the presence of 1000 nM interfering substance (%Δ).

Aptamer	Fipronil added (nM)	Interferant added	Interferant concentration (nM)	Deviation on the sensor signal after interference agent (%Δ)	Fipronil found (nM)	RE %
Anti-FIP1	10	BSA	1000	0.65	10.42 ± 0.02	4.2
	10	ETH	1000	1.09	10.73 ± 0.02	7.3
Anti-FIP2	10	BSA	1000	0.81	10.59 ± 0.01	5.9
	10	ETH	1000	1.18	10.86 ± 0.01	8.6
Anti-FIP1	1000	BSA	1000	0.67	1077.22 ± 0.02	7.7
	1000	ETH	1000	1.03	1120.47 ± 0.02	12.0
Anti-FIP2	1000	BSA	1000	0.58	1069.30 ± 0.01	6.9
	1000	ETH	1000	1.03	1126.96 ± 0.01	12.7

Table 4
Accuracy and precision results for Anti-FIP1 and Anti-FIP2 (experiments conducted in 5 replicates and presented as mean value with standard deviation ± σ where applicable).

Aptamer	Fipronil added (nM)	Inter-day			Intra-day*		
		Found (nM)	Accuracy %	Precision %	Found (nM)	Accuracy %	Precision %
Anti-FIP1	10	9.69 ± 0.018	−3.10	0.18	10.69 ± 0.022	+6.9	0.22
	1000	914.65 ± 0.019	−8.54	0.002	1062.07 ± 0.028	+6.2	0.003
Anti-FIP2	10	10.03 ± 0.01	+0.3	0.10	10.93 ± 0.01	+9.3	0.1
	1000	988.35 ± 0.01	−1.17	0.001	1095.71 ± 0.02	+9.6	0.002

* Five consecutive days.

to +0.3 %, while the inter-day accuracy was found between +9.3 % and +9.6 %. There was no significant variability observed in accuracy and precision across all measurements. No clear systematic bias was observed in the accuracy measurements, with accuracies ranging from −8.5 % to +9.6 % for both aptamers.

6. Food samples

Both aptamers were used to detect fipronil in real samples through spiking into locally sourced egg and cereal (wheat) samples. After sample preparation steps, samples spiked with three different concentrations (1 nM, 100 nM, and 1000 nM fipronil) were tested (Table 5).

For the Anti-FIP1 aptamer, the recovery deviation in egg samples ranged from −2.61 % to 5.53 %. In cereal samples, the recovery was between −8.94 % and 5.44 %. When the Anti-FIP2 aptamer was used, the recovery in egg samples ranged from −2.34 % to 5.05 %, while in cereal samples, it was between −0.33 % and 3.58 %. The recovery values fall within the accuracy deviation limits of the spectrophotometric aptasensors, with a recovery of <±10 %.

Since measurements were made on real samples using the spiking method and no positive systematic bias was observed, it was assumed that fipronil was not present in the samples taken. Considering the detection limit of both aptamers and the recovery values from real samples, it can be seen that fipronil can be successfully detected in food samples.

Table 5
Analytical recovery data of sensors from egg and cereal products, experiments were repeated 3 times and presented as the average of the results.

	Samples	Added (nM)	Detected (nM)	RE (%)
Anti-FIP1	Egg	1.00	1.06 ± 0.02	5.53
		100.0	97.39 ± 0.03	−2.61
		1000	1034.57 ± 0.03	3.46
	Grain	1.00	0.97 ± 0.02	−3.09
		100.0	105.44 ± 0.02	5.44
		1000	910.58 ± 0.03	−8.94
Anti-FIP2	Egg	1.00	1.05 ± 0.01	5.05
		100.0	103.83 ± 0.01	3.83
		1000	997.66 ± 0.01	−2.34
	Grain	1.00	0.99 ± 0.01	−0.33
		100.0	99.63 ± 0.01	−0.37
		1000	1035.78 ± 0.01	3.58

7. Conclusion

Due to its toxicity and long-lasting presence, fipronil and its metabolites pose a danger in food samples. In this study, we report highly sensitive aptasensor platforms for fipronil detection using the SE method, as it is sensitive to molecular accumulation on the substrate material, as measured by Δ (phase shift) values. The LOD values for both aptamers in the buffer solution were quite promising, reaching 33.7 pM for Anti-FIP1 and 24.9 pM for Anti-FIP2. These figures are well within the range of other fipronil detection methods summarized in Table 1, reported in the literature. Moreover, due to the extensive molecule cocktail used in the negative selection at the aptamer selection stage, the specificity of the aptamers to BSA and ETH in the SE sensor structure approached the limit of repeatability. Since its analytical performance in terms of sensitivity and selectivity are remarkable, it can be concluded that the proposed SE method is a good candidate for fipronil detection even from a complex media. However, since it's a sophisticated instrument, miniaturization of SE to form a handheld or portable device for on-site measurements is not possible. Nonetheless, measurements in the drop-measure format, which do not require any additional labeling, coupled with the use of multiple manufactured SE sensor chips, could allow for high-throughput analysis in the laboratory environment. Especially considering that only meeting the mass transfer-complex formation rate is sufficient in terms of analysis time, yielding results within a maximum of 30 min can also be considered an advantage. In conclusion, the proposed ellipsometric-based aptasensors have shown

promising results for the detection of fipronil in real samples.

CRediT authorship contribution statement

Arzu Keske: Resources, Investigation. **Mustafa Oguzhan Caglayan:** Writing – original draft, Supervision, Conceptualization. **Zafer Üstündağ:** Writing – original draft, Project administration, Methodology, Investigation, Funding acquisition.

Declaration of competing interest

The authors declare that they have no known competing financial interests or personal relationships that could have appeared to influence the work reported in this paper.

Data availability

No data was used for the research described in the article.

Acknowledgments

This work was financially supported by the Scientific and Technological Research Council of Turkey (TÜBİTAK) under Grant No: 120Z253. Authors appreciate and gratefully acknowledge this financial support.

Appendix A. Supplementary data

Supplementary data to this article can be found online at https://doi.org/10.1016/j.microc.2024.110953.

References

[1] N. Simon-Delso, V. Amaral-Rogers, L.P. Belzunces, J.M. Bonmatin, M. Chagnon, C. Downs, L. Furlan, D.W. Gibbons, C. Giorio, V. Girolami, D. Goulson, D. P. Kreutzweiser, C.H. Krupke, M. Liess, E. Long, M. McField, P. Mineau, E. A. Mitchell, C.A. Morrissey, D.A. Noome, L. Pisa, J. Settele, J.D. Stark, A. Tapparo, H. Van Dyck, J. Van Praagh, J.P. Van der Sluijs, P.R. Whitehorn, M. Wiemers, Systemic insecticides (neonicotinoids and fipronil): trends, uses, mode of action and metabolites, Environ. Sci. Pollut. Res. Int. 22 (2015) 5–34.
[2] C.C. Tingle, J.A. Rother, C.F. Dewhurst, S. Lauer, W.J. King, Fipronil: environmental fate, ecotoxicology, and human health concerns, Rev. Environ. Contam. Toxicol. 176 (2003) 1–66.
[3] G.S. Barbara, C. Zube, J. Rybak, M. Gauthier, B. Grünewald, Acetylcholine, GABA and glutamate induce ionic currents in cultured antennal lobe neurons of the honeybee, Apis mellifera, J. Compar. Physiol. A 191 (2005) 823–836.
[4] J.E. Casida, Neonicotinoid metabolism: compounds, substituents, pathways, enzymes, organisms, and relevance, J. Agric. Food Chem. 59 (2011) 2923–2931.
[5] D. Hainzl, L.M. Cole, J.E. Casida, Mechanisms for selective toxicity of fipronil insecticide and its sulfone metabolite and desulfinyl photoproduct, Chem. Res. Toxicol. 11 (1998) 1529–1535.
[6] D. Hainzl, J.E. Casida, Fipronil insecticide: novel photochemical desulfinylation with retention of neurotoxicity, Proc. Natl. Acad. Sci. U.S.A. 93 (1996) 12764–12767.
[7] P. Caboni, R.E. Sammelson, J.E. Casida, Phenylpyrazole insecticide photochemistry, metabolism, and GABAergic action: ethiprole compared with fipronil, J. Agric. Food Chem. 51 (2003) 7055–7061.
[8] T.M. DeLorey, A. Handforth, S.G. Anagnostaras, G.E. Homanics, B.A. Minassian, A. Asatourian, M.S. Fanselow, A. Delgado-Escueta, G.D. Ellison, R.W. Olsen, Mice lacking the beta3 subunit of the GABAA receptor have the epilepsy phenotype and many of the behavioral characteristics of Angelman syndrome, J. Neurosci. 18 (1998) 8505–8514.
[9] N. Vasylieva, K.C. Ahn, B. Barnych, S.J. Gee, B.D. Hammock, Development of an immunoassay for the detection of the phenylpyrazole insecticide fipronil, Environ. Sci. Technol. 49 (2015) 10038–10047.
[10] F. Mohamed, L. Senarathna, A. Percy, M. Abeyewardene, G. Eaglesham, R. Cheng, S. Azher, A. Hittarage, W. Dissanayake, M.H. Sheriff, W. Davies, N.A. Buckley, M. Eddleston, Acute human self-poisoning with the N-phenylpyrazole insecticide fipronil–a GABAA-gated chloride channel blocker, J. Toxicol. Clin. Toxicol. 42 (2004) 955–963.
[11] A. Bobé, P. Meallier, J.-F. Cooper, C.M. Coste, Kinetics and mechanisms of abiotic degradation of fipronil (hydrolysis and photolysis), J. Agric. Food Chem. 46 (1998) 2834–2839.
[12] N.D. Chau, Z. Sebesvari, W. Amelung, F.G. Renaud, Pesticide pollution of multiple drinking water sources in the Mekong Delta, Vietnam: evidence from two provinces, Environ. Sci. Pollut. Res. Int. 22 (2015) 9042–9058.
[13] J.M. Bonmatin, C. Giorio, V. Girolami, D. Goulson, D.P. Kreutzweiser, C. Krupke, M. Liess, E. Long, M. Marzaro, E.A. Mitchell, D.A. Noome, N. Simon-Delso, A. Tapparo, Environmental fate and exposure; neonicotinoids and fipronil, Environ. Sci. Pollut. Res. Int. 22 (2015) 35–67.
[14] W.W. Stone, R.J. Gilliom, K.R. Ryberg, Pesticides in U.S. streams and rivers: occurrence and trends during 1992–2011, Environ. Sci. Tech. 48 (2014) 11025–11030.
[15] L. Paolini, N. Hausser, T. Zhang, Chiral resolution of the insecticide fipronil enantiomers and the simultaneous determination of its major transformation products by high-performance liquid chromatography interfaced with mass spectrometry, Chirality 34 (2022) 473–483.
[16] V.A.A. Pastore, F.A. Santos, M.A.G. Lana, G.R. Silva, T.C. Figueiredo, D.C.S. Assis, S.V. Cançado, Development and validation of a multiresidue method for the determination of macrocyclic lactones, monensin, and fipronil in bovine liver by UHPLC-MS/MS using a QuEChERS extraction, Food Anal. Methods 15 (2022) 3177–3188.
[17] R. Rao Pasupuleti, Y.-J. Ku, T.-Y. Tsai, H.-T. Hua, Y.-C. Lin, J. Shiea, P.-C. Huang, G. Andaluri, V.K. Ponnusamy, Novel fast pesticides extraction (FaPEx) strategy coupled with UHPLC-MS/MS for rapid monitoring of emerging pollutant fipronil and its metabolite in food and environmental samples, Environ. Res. 217 (2023) 114823.
[18] L. Qu, X. Qi, L. Zhao, Y. Zhang, R. Zhuge, Z. Hao, C. Liu, Development, validation, and use of a monitoring method for fipronil and its metabolites in chicken eggs by QuEChERS with online-SPE-LC-Q/Orbitrap analysis, Rapid Commun. Mass Spectrometry 37 (2023) e9518.
[19] R.P. Rathnasekara, A.M. Rustum, Simultaneous determination of praziquantel, fipronil, eprinomectin, (S)-methoprene, their key related substances and butylated hydroxytoluene (BHT) in a topical veterinary drug product by a single stability indicating high performance liquid chromatography method, J. Pharm. Biomed. Anal. 238 (2024) 115805.
[20] E. Torabi, K. Talebi, A.A. Pourbabaee, M. Homayoonzadeh, M.J. Ghamari, S. Ebrahimi, N. Faridy, Optimizing the QuEChERS method for efficient monitoring of fipronil, thiobencarb, and cartap residues in paddy soils with varying properties, Environ. Monit. Assess. 196 (2024) 125.
[21] C. Wang, Y. Lin, Y. Wang, T.-F. Jiang, Z. Lv, Determination of fipronil and its metabolites in chicken egg by dispersive liquid–liquid microextraction with 19F quantitative nuclear magnetic resonance spectroscopy, Microchem. J. 160 (2021) 105547.
[22] K.-H. Wu, W.-C. Huang, S.-C. Chang, C.-H. Kao, R.-H. Shyu, Preparation of competitive immunochromatographic assay for detection of residual fipronil in urine and food samples, Mater. Express 11 (2021) 63–72.
[23] J. Yao, Z. Wang, L. Guo, X. Xu, L. Liu, H. Kuang, C. Xu, Lateral flow immunoassay for the simultaneous detection of fipronil and its metabolites in food samples, Food Chem. 356 (2021) 129710.
[24] X. Zhang, Y. Zhou, X. Huang, X. Hu, X. Huang, L. Yin, Q. Huang, Y. Wen, B. Li, J. Shi, X. Zou, Switchable aptamer-fueled colorimetric sensing toward agricultural fipronil exposure sensitized with affiliative metal-organic framework, Food Chem. 407 (2023) 135115.
[25] J. Yoo, S. Han, B. Park, S. Sonwal, M. Alhammadi, E. Kim, S. Aliya, E.-S. Lee, T.-J. Jeon, M.-H. Oh, Y.S. Huh, Highly specific peptide-mediated cuvette-form localized surface plasmon resonance (LSPR)-based fipronil detection in egg, Biosensors 12 (2022) 914.
[26] J. Yin, X. Chen, Z. Chen, Quenched electrochemiluminescence sensor of ZnO@g-C3N4 modified glassy carbon electrode for fipronil determination, Microchem. J. 145 (2019) 295–300.
[27] M. Nurdin, Z. Arham, S. Rahayu, L.O. Agus Salim, M. Maulidiyah, Electroanalytical performance of graphene paste electrode modified Al(III)-TiO2 nanocomposites in fipronil solution, Jurnal Rekayasa Kimia & Lingkungan 15 (2020) 71–78.
[28] S. Kumar, N. Vasylieva, V. Singh, B. Hammock, S.G. Singh, A. Facile, Sensitive and rapid sensing platform based on CoZnO for detection of fipronil; an environmental toxin, Electroanalysis 32 (2020) 2056–2064.
[29] M. Nurdin, O.A. Prabowo, Z. Arham, D. Wibowo, M. Maulidiyah, S.K.M. Saad, A. A. Umar, Highly sensitive fipronil pesticide detection on ilmenite (FeO.TiO2)-carbon paste composite electrode, Surf. Interfaces 16 (2019) 108–113.
[30] M. Nurdin, Z. Arham, W.O. Irna, M. Maulidiyah, K. Kurniawan, L.O.A. Salim, I. Irwan, A.A. Umar, Enhanced-charge transfer over molecularly imprinted polyaniline modified graphene/TiO2 nanocomposite electrode for highly selective detection of fipronil insecticide, Mater. Sci. Semicond. Process. 151 (2022) 106994.
[31] H. Huang, C. Zhang, J. Zhou, D. Wei, T. Ma, W. Guo, X. Liu, S. Li, Y. Deng, Label-free aptasensor for detection of fipronil based on black phosphorus nanosheets, Biosensors 12 (2022) 775.
[32] R. Svigelj, N. Dassi, A. Gorassini, R. Toniolo, A smartphone aptasensor for fipronil detection in honey samples, Anal. Bioanal. Chem. 416 (2024) 397–405.
[33] W.-C. Huang, Y.-N. Hsiung, C.-L. Li, An electrochemical immunosensor based on a carboxylated multiwalled carbon nanotube-silver nanoparticle-chitosan functional layer for the detection of fipronil, Nanoscale Adv. 5 (2023) 6548–6559.
[34] S. El-Akaad, R. Morozov, M. Golovin, O. Bol'shakov, S. De Saeger, N. Beloglazova, A novel electrochemical sensor for the detection of fipronil and its toxic metabolite fipronil sulfone using TiO2-polytriazine imide submicrostructured composite as an efficient electrocatalyst, Talanta 238 (2022) 123025.
[35] M. Maulidiyah, T. Azis, L. Lindayani, D. Wibowo, L.O.A. Salim, A. Aladin, M. Nurdin, Sol-gel TiO2/carbon paste electrode nanocomposites for electrochemical-assisted sensing of fipronil pesticide, J. Electrochem. Sci. Technol. 10 (2019) 394–401.

[36] J.A. Diniz, L.L. Okumura, A. Filomena de Souza Silva, A.F. Oliveira, A. Gurgel, P. A. Liberato, H. Aleixo, J.G. Silva, Study and voltammetric determination of fipronil in bovine lactose-free milk by differential pulse voltammetry using a carbon paste electrode, Anal. Methods 15 (2023) 1517–1526.
[37] K. Wang, N. Vasylieva, D. Wan, D.A. Eads, J. Yang, T. Tretten, B. Barnych, J. Li, Q. X. Li, S.J. Gee, B.D. Hammock, T. Xu, Quantitative detection of fipronil and fipronil-sulfone in sera of black-tailed prairie dogs and rats after oral exposure to fipronil by camel single-domain antibody-based immunoassays, Anal. Chem. 91 (2019) 1532–1540.
[38] X. Liu, C. Yan, J. Dong, X. Yu, D. Xu, Poly- and monoclonal antibody-based ELISAs for fipronil, J. Agric. Food Chem. 55 (2007) 226–230.
[39] J. Liu, Y. Wu, C. Liu, Y. Cai, R. Zhang, Y. Lu, Development of an ic-ELISA and a TRFICA for the detection of fipronil with a new hapten design, J. Food Meas. Charact. 18 (2024) 2561–2572.
[40] K.L. Hong, L.J. Sooter, In vitro selection of a single-stranded DNA molecular recognition element against the pesticide fipronil and sensitive detection in river water, Int. J. Mol. Sci. 19 (2018) 85.
[41] C. Yang, L. Wang, Z. Zhang, Y. Chen, Q. Deng, S. Wang, Fluorometric determination of fipronil by integrating the advantages of molecularly imprinted silica and carbon quantum dots, Mikrochim. Acta (2019) 12.
[42] T.-Y. Kim, J.W. Lim, M.-C. Lim, N.-E. Song, M.-A. Woo, Aptamer-based fluorescent assay for simple and sensitive detection of fipronil in liquid eggs, Biotechnol. Bioprocess. Eng. 25 (2020) 246–254.
[43] K.H. Trinh, U.S. Kadam, S. Rampogu, Y. Cho, K.-A. Yang, C.H. Kang, K.-W. Lee, K. O. Lee, W.S. Chung, J.C. Hong, Development of novel fluorescence-based and label-free noncanonical G4-quadruplex-like DNA biosensor for facile, specific, and ultrasensitive detection of fipronil, J. Hazard. Mater. 427 (2022) 127939.
[44] J. Zhang, T. Feng, J. Zhang, N. Liang, L. Zhao, Fluorescence assay for the sensitive detection of fipronil based on an "on–off" oxidized SWCNH/aptamer sensor, Anal. Methods 13 (2021) 3282–3291.
[45] L. Yin, X. Hu, M. Hao, J. Shi, X. Zou, K.D. Dusabe, Upconversion nanoparticles-based background-free selective fluorescence sensor developed for immunoassay of fipronil pesticide, J. Food Meas. Charact. 17 (2023) 3125–3133.
[46] Y. Zhang, X. Bai, C. Lv, Y. Fang, Y. Tang, H. Jiang, G. Huang, An aptasensor based on the fluorescence resonance energy transfer of nitrogen-doped carbon quantum dots and graphene oxide to detect fipronil in eggs, Eur. Food Res. Technol. 249 (2023) 2887–2895.
[47] D. Song, J. Liu, W. Xu, X. Han, H. Wang, Y. Zhuo, C. Li, F. Long, On-site rapid and simultaneous detection of acetamiprid and fipronil using a dual-fluorescence lab-on-fiber biosensor, Microchim. Acta 189 (2022) 234.
[48] Y. Li, W. Xu, J. Liu, E. Zhang, H. Li, Y. Zhang, J. Zhang, C. Li, X. Zhang, Rapid and sensitive on-site detection of fipronil in foods using evanescent wave fluorescent immunosensor, Chemosensors 11 (2023) 578.
[49] X. Liu, J. Song, X. Zhang, S. Huang, B. Zhao, X. Feng, A highly selective and sensitive europium-organic framework sensor for the fluorescence detection of fipronil in tea, Food Chem. 413 (2023) 135639.
[50] Q. Zhao, S.W. Yue, Y.L. Zhou, J.J. Yang, Determination of fipronil and its metabolites in environmental water samples by meltblown nonwoven fabric-based solid-phase extraction combined with gas chromatography-electron capture detection, J. Sep. Sci. 45 (2022) 2663–2674.
[51] Y.-L. Zhou, S.-W. Yue, B.-W. Cheng, Q. Zhao, Determination of fipronil and its metabolites in edible oil by pollen based solid-phase extraction combined with gas chromatography-electron capture detection, Food Chem. 377 (2022) 132021.
[52] X.-T. Peng, Y.-N. Li, H. Xia, L.-J. Peng, Y.-Q. Feng, Rapid and sensitive detection of fipronil and its metabolites in edible oils by solid-phase extraction based on humic acid bonded silica combined with gas chromatography with electron capture detection, J. Sep. Sci. 39 (2016) 2196–2203.
[53] E. Bichon, C.A. Richard, B. Le Bizec, Development and validation of a method for fipronil residue determination in ovine plasma using 96-well plate solid-phase extraction and gas chromatography-tandem mass spectrometry, J. Chromatogr. A 1201 (2008) 91–99.
[54] J.L. Vílchez, A. Prieto, L. Araujo, A. Navalón, Determination of fipronil by solid-phase microextraction and gas chromatography-mass spectrometry, J. Chromatogr. A 919 (2001) 215–221.
[55] J. Ma, X. Lu, Y. Xia, F. Yan, Determination of pyrazole and pyrrole pesticides in environmental water samples by solid-phase extraction using multi-walled carbon nanotubes as adsorbent coupled with high-performance liquid chromatography, J. Chromatogr. Sci. 53 (2014) 380–384.
[56] Q. Zhang, X. Wang, X. Wang, H. Guo, G. Chen, Y. Shan, W. Fang, Development of a pass-through SPE cartridge for the rapid determination of fipronil and its metabolites in chicken eggs by LC-MS/MS, Food Anal. Methods 14 (2021) 922–932.
[57] X. Li, J. Chen, X. He, Z. Wang, D. Wu, X. Zheng, L. Zheng, B. Wang, Simultaneous determination of neonicotinoids and fipronil and its metabolites in environmental water from coastal bay using disk-based solid-phase extraction and high-performance liquid chromatography–tandem mass spectrometry, Chemosphere 234 (2019) 224–231.
[58] Y. Zhao, R. Boukherroub, G. Xu, H. Li, R.-S. Zhao, Q. Wei, X. Yu, X. Chen, Au@BN-enhanced laser desorption/ionization mass spectrometry and imaging for determination of fipronil and its metabolites in food and biological samples, Food Chem. 418 (2023) 135935.
[59] S.-L. Yang, J.-N. Lu, S.-J. Zhang, C.-X. Zhang, Q.-L. Wang, 2D europium coordination polymer as a regenerable fluorescence probe for efficiently detecting fipronil, Analyst 143 (2018) 4901–4906.
[60] Q. Tu, M.E. Hickey, T. Yang, S. Gao, Q. Zhang, Y. Qu, X. Du, J. Wang, L. He, A simple and rapid method for detecting the pesticide fipronil on egg shells and in liquid eggs by Raman microscopy, Food Control 96 (2019) 16–21.
[61] N.H. Ly, T.H. Nguyen, N.Đ. Nghi, Y.-H. Kim, S.-W. Joo, Surface-enhanced Raman scattering detection of fipronil pesticide adsorbed on silver nanoparticles, Sensors 19 (2019) 1355.
[62] M. Muhammad, G. Yao, J. Zhong, K. Chao, M.H. Aziz, Q. Huang, A facile and label-free SERS approach for inspection of fipronil in chicken eggs using SiO2@Au core/shell nanoparticles, Talanta 207 (2020) 120324.
[63] H.L. Lai, S. Ghosh, S. Chattopadhyay, The detection of fipronil residue in egg on layered gold nanorod–graphene oxide-based 3D SERS substrate, Analyst 146 (2021) 3557–3567.
[64] C. Sun, L. Wang, N. Guo, R. Hu, L. Ye, Z. Hu, J. Ding, Research on a three-dimensional SERS substrate based on a CNTs/Ag@Au/SiO2 composite for detection of fipronil and imidacloprid pesticides, Anal. Methods 15 (2023) 4494–4505.
[65] Y. Liu, Z. Qin, A. Liang, G. Wen, Z. Jiang, A new N/Fe doped carbon dot nanosurface molecularly imprinted polymethacrylate nanoprobe for trace fipronil with SERS/RRS dimode technique, Talanta 269 (2024) 125417.
[66] K. Han, J. Hua, Q. Zhang, Y. Gao, X. Liu, J. Cao, N. Huo, Multi-residue analysis of fipronil and its metabolites in eggs by SinChERS-based UHPLC-MS/MS, Food Sci. Anim. Resour. 41 (2021) 59–70.
[67] D. Castilla-Fernández, D. Moreno-González, M.C. Murillo-Cruz, J.F. García-Reyes, A. Molina-Díaz, Appraisal of different clean-up strategies for the determination of fipronil and its metabolites in eggs by UHPLC-MS/MS, Microchem. J. 166 (2021) 106275.
[68] Y. Zhao, X.-L. Bai, Y.-M. Liu, X. Liao, Determination of fipronil and its metabolites in egg samples by UHPLC coupled with Q-Exactive high resolution mass spectrometry after magnetic solid-phase extraction, Microchem. J. 169 (2021) 106540.
[69] A.D. Ellington, J.W. Szostak, In vitro selection of RNA molecules that bind specific ligands, Nature 346 (1990) 818–822.
[70] C. Tuerk, L. Gold, Systematic evolution of ligands by exponential enrichment: RNA ligands to bacteriophage T4 DNA polymerase, Science (New York, N.Y.) 249 (1990) 505–510.
[71] L.F. Yang, M. Ling, N. Kacherovsky, S.H. Pun, Aptamers 101: aptamer discovery and in vitro applications in biosensors and separations, Chem. Sci. 14 (2023) 4961–4978.
[72] M. Poksinski, H. Arwin, In situ monitoring of metal surfaces exposed to milk using total internal reflection ellipsometry, Sens. Actuators B 94 (2003) 247–252.
[73] R. Naraoka, K. Kajikawa, Phase detection of surface plasmon resonance using rotating analyzer method, Sens. Actuators B 107 (2005) 952–956.
[74] A. Nabok, A. Tsargorodskaya, M.K. Mustafa, I. Székács, N.F. Starodub, A. Székács, Detection of low molecular weight toxins using an optical phase method of ellipsometry, Sens. Actuators B 154 (2011) 232–237.
[75] M.O. Caglayan, Aptamer-based ellipsometric sensor for ultrasensitive determination of aminoglycoside group antibiotics from dairy products, J. Sci. Food Agric. 100 (2020) 3386–3393.
[76] M.O. Caglayan, Z. Üstündağ, Spectrophotometric ellipsometry based Tat-protein RNA-aptasensor for HIV-1 diagnosis, Spectrochim. Acta A Mol. Biomol. Spectrosc. 227 (2020) 117748.
[77] A. Keske, A. Atar, Ü. Lknur, C.M. Oguzhan, Detection of influenza a by surface plasmon resonance enhanced total internal reflection ellipsometry, J. Comput. Theor. Nanosci. 11 (2014) 981–986.
[78] M.O. Caglayan, Plasmon resonance-enhanced internal reflection ellipsometry for the trace detection of mercuric ion, Int. J. Environ. Sci. Technol. 15 (2018) 909–914.
[79] M.O. Caglayan, Z. Üstündağ, Detection of zearalenone in an aptamer assay using attenuated internal reflection ellipsometry and it's cereal sample applications, Food Chem. Toxicol. 136 (2020) 111081.
[80] R. Lenigk, M. Carles, N.Y. Ip, N.J. Sucher, Surface characterization of a silicon-chip-based DNA microarray, Langmuir 17 (2001) 2497–2501.
[81] X. Li, H. Li, W. Ma, Z. Guo, X. Li, S. Song, H. Tang, X. Li, Q. Zhang, Development of precise GC-EI-MS method to determine the residual fipronil and its metabolites in chicken egg, Food Chem. 281 (2019) 85–90.
[82] J. Le Faouder, E. Bichon, P. Brunschwig, R. Landelle, F. Andre, B. Le Bizec, Transfer assessment of fipronil residues from feed to cow milk, Talanta 73 (2007) 710–717.
[83] A. Duhan, B. Kumari, S. Duhan, Determination of residues of fipronil and its metabolites in cauliflower by using gas chromatography-tandem mass spectrometry, Bull. Environ. Contam. Toxicol. 94 (2015) 260–266.
[84] M. Ben Haddada, J. Blanchard, S. Casale, J.-M. Krafft, A. Vallée, C. Méthivier, S. Boujday, Optimizing the immobilization of gold nanoparticles on functionalized silicon surfaces: amine- vs thiol-terminated silane, Gold Bull. 46 (2013) 335–341.
[85] M. Zuker, Mfold web server for nucleic acid folding and hybridization prediction, Nucl. Acids Res. 31 (2003) 3406–3415.